0026-895X/11/7904-701–709$20.00
MOLECULAR PHARMACOLOGY
Vol. 79, No. 4
70177/3677692
Mol Pharmacol 79:701–709, 2011
Printed in U.S.A.

Helix 8 of the M_1 Muscarinic Acetylcholine Receptor: Scanning Mutagenesis Delineates a G Protein Recognition Site[S]

Robert G. Kaye,[1] José W. Saldanha, Zhi-Liang Lu, and Edward C. Hulme

Divisions of Physical Biochemistry (R.G.K., E.C.H.) and Mathematical Biology (J.W.S.), MRC National Institute for Medical Research, Mill Hill, London, United Kingdom; and Department of Biological Sciences, Xi'an Jiaotong-Liverpool University, Suzhou, People's Republic of China (Z.-L.L.)

Received November 26, 2010; accepted January 19, 2011

ABSTRACT

We have used alanine-scanning mutagenesis followed by functional expression and molecular modeling to analyze the roles of the 14 residues, Asn422 to Cys435, C-terminal to transmembrane (TM) helix 7 of the M_1 muscarinic acetylcholine receptor. The results suggest that they form an eighth (H8) helix, associated with the cytoplasmic surface of the cell membrane in the active state of the receptor. We suggest that the amide side chain of Asn422 may act as a cap to the C terminus of TM7, stabilizing its junction with H8, whereas the side chain of Phe429 may restrict the relative movements of H8 and the C terminus of TM7 in the inactive ground state of the receptor. We have identified four residues, Phe425, Arg426, Thr428, and Leu432, which are important for G protein binding and signaling. These may form a docking site for the C-terminal helix of the G protein α subunit, and collaborate with G protein recognition residues elsewhere in the cytoplasmic domain of the receptor to form a coherent surface for G protein binding in the activated state of the receptor.

Introduction

A fourth intracellular loop (ICL) was proposed to exist in the prototypical G protein-coupled receptor rhodopsin after the realization that two cysteine residues in its C-terminal sequence are palmitoylated and therefore membrane-anchored (Ovchinnikov et al., 1988). Sequence homology showed that a membrane-anchored ICL4 was likely to be common in GPCRs (Milligan et al., 1995), including muscarinic acetylcholine receptors (mAChRs) (Hulme et al., 1990).

Peptide competition studies were the first to show that ICL4 of rhodopsin participates in G-protein recognition (König et al., 1989), whereas cysteine substitution mutagenesis followed by probing with a spin label indicated its involvement in the conformational change induced by photoactivation (Resek et al., 1993). More detailed investigation showed that this conformational rearrangement occurred within a well organized tertiary structure (Altenbach et al., 1999; Cai et al., 1999) and, as a byproduct, identified three amino acids (Asn7.57, Phe7.60, and Phe7.64, using the Ballesteros-Weinstein standard numbering convention) whose cysteine substitution inhibited G protein activation. Solution of the crystal structure of rhodopsin showed that ICL4 forms a three-turn helix (H8) that is attached to transmembrane (TM) helix 7 by a short linker and is anchored to the cytoplasmic surface of the cell membrane by the palmitic acid moieties (Palczewski et al., 2000). A stacking interaction occurs between the side chains of Phe7.60 (H8) and Tyr7.53 (TM7), which helps to constrain inactive rhodopsin to the ground state and is broken during activation (Scheerer et al., 2008).Mutational studies indicated that the structural integrity of both of these side chains is important for G-protein binding (Fritze et al., 2003). H8 participates in the structural change that accompanies the activation of rhodopsin (Hoersch et al., 2008).

H8 has also been identified in the crystal structure of squid rhodopsin (Murakami and Kouyama, 2008) and in the structures of the β_2, β_1-adrenergic and A_{2A}-adenosine receptors (Cherezov et al., 2007; Jaakola et al., 2008; Warne et al., 2008) although, interestingly, not in the CXCR4 receptor, which lacks the F(R/K)xx(F/L)xxH consensus sequence (Wu et al., 2010). Mutational studies on a variety of receptors

This work was funded by the Medical Research Council, United Kingdom [Grants U117532184, U117581331]. R.K. received a Medical Research Council Sandwich Student Placement for 2009–2010.

[1] Current affiliation: Department of Cell Physiology and Pharmacology, University of Leicester, Leicester, United Kingdom.

Article, publication date, and citation information can be found at http://molpharm.aspetjournals.org.
doi:10.1124/mol.110.070177.

[S] The online version of this article (available at http://molpharm.aspetjournals.org) contains supplemental material.

ABBREVIATIONS: ICL, intracellular loop; mAChR, muscarinic acetylcholine receptor; ACh, acetylcholine; Pilo, pilocarpine; TM, transmembrane domain; ECL, extracellular loop; H8, helix 8; NMS, (−)-*N*-methyl scopolamine; PI, phosphoinositide; PDB, Protein Data Bank; GPCR, G protein-coupled receptor; WT, wild type.

have supported the general involvement of H8 in G protein recognition (O'Dowd et al., 1989; Sano et al., 1997; Okuno et al., 2003; Delos Santos et al., 2006; Swift et al., 2006; Anavi-Goffer et al., 2007) or conformational switching (Prioleau et al., 2002). H8, in particular, a dileucine motif toward the C-terminal end, also has been implicated in control of receptor expression (Sawyer et al., 2010) and is suggested to be part of a dimerization interface involving TM1 (Fung et al., 2009). In the M_3 mAChR, cysteine substitution and disulfide cross-linking studies indicated that the N-terminal part of H8 moves away from TM1 during agonist activation (Li et al., 2007) and that residues in H8 can undergo both agonist-independent and -dependent cross-linking to $G_q\alpha$ (Hu et al., 2010).

Despite this range of studies, there has been no report of a systematic and comparative evaluation of the role of residues in H8 in regulating the ligand-dependent activation of a GPCR. In this report, we have applied alanine-scanning mutagenesis to residues Asn422 to Cys435 in the putative H8 sequence of the M_1 mAChR. Their location is indicated in the scheme shown in Fig. 6a. We have identified four amino acids—Phe425 (7.60), Arg426 (7.61), Thr428 (7.63), and Leu432 (7.67)—whose mutagenic phenotype suggests that they participate in G protein activation. They may collaborate with residues in the C-terminal extensions of TM5 and TM6, contributing to a coherent surface for G-protein binding in the activated state of the receptor.

Materials and Methods

The majority of procedures were as described in a recent publication (Lebon et al., 2009).

Materials. (−)-*N*-[^{3}H]Methylscopolamine (82, 84 Ci/mmol) was purchased from GE Healthcare (Chalfont St. Giles, Buckinghamshire, UK). [*myo*-D-^{3}H]Inositol (20 Ci/mmol) was from PerkinElmer Life and Analytical Sciences (Waltham, MA). (−)-Scopolamine methyl bromide, acetylcholine (2-acetyloxy-*N*,*N*,*N*-trimethylethanaminium) bromide, and pilocarpine [(3*S*,4*R*)-3-ethyl-4-[(3-methylimidazol-4-yl)methyl]oxolan-2-one] were from Sigma-Aldrich (Gillingham, UK).

DNA and Expression. Residues Asn422 to Cys435 of the rat M_1 mAChR, cloned in the pCD expression vector, were mutated to alanine (GCG or GCC) by a polymerase chain reaction procedure; Ala423 was mutated to glycine (GGC). Mutant sequences were verified by di-deoxy sequencing (Beckman Coulter, Fullerton, CA) before transient expression in COS-7 cells grown in minimal essential medium-α supplemented with 10% newborn calf serum and 1% glutamate plus antibiotics at 37°C in 5% CO_2 (Lebon et al., 2009). The medium was changed after 24 h, and the cells were grown for a further 48 h before assay or harvesting. In some experiments, the media were supplemented with atropine (10^{-6} M) after 24 h to rescue the low-expressing mutant N422A, as described previously (Lu and Hulme, 1999; Bee and Hulme, 2007). Membrane protein concentrations were measured using the micro-BCA assay with bovine serum albumin as standard.

Radioligand Binding Assays: Membranes. Radioligand binding assays were performed on membrane preparations from transfected COS-7 cells as described previously (Lebon et al., 2009). In brief, radioligand saturation assays were performed using [^{3}H]NMS concentrations ranging from 0.1× to 30× K_d (10^{-11} M–3×10^{-9} M) using 1 ml of reaction volumes in 96 × 2 ml reaction blocks (Masterblock, Greiner Bio-One, Monroe, NC). Each measurement of ACh inhibition of [^{3}H]NMS binding was conducted using three concentrations of [^{3}H]NMS, equivalent to 0.1, 2, and 10 times the measured K_d for [^{3}H]NMS. Nonspecific binding was defined using 10^{-5} M unlabeled (−)-scopolamine. Receptor concentrations ranged from 15 to 40 fmol/ml. Each point was determined in quadruplicate. The buffer consisted of 20 mM sodium-HEPES, 0.1 M NaCl, and 1 mM $MgCl_2$, pH 7.5. For equilibrium binding assays, the incubation time was 2 h at 30°C. For measurements of [^{3}H]NMS dissociation, membranes were preincubated with 5×10^{-10} M [^{3}H]NMS for 60 min before initiation of dissociation by adding (−)-scopolamine (10^{-5} M) using a reverse time course strategy resulting in dissociation times ranging from 1 to 60 min. Binding reactions were terminated by rapid filtration onto Wallac 96-Printed GF/B filters (PerkinElmer Life and Analytical Sciences) using a TOMTEC Harvester 96, MACH III (Tomtec, Hamden, CT), followed by three washes with ice-cold water. The filters were dried, processed by melting on of Meltilex B/HS filter sheets, and counted in a normalized, calibrated 1450 MicroBeta TriLux counter (5 min per sample; PerkinElmer Life and Analytical Sciences).

Radioligand Binding Assays: Whole Cells. Transfected COS-7 cells were grown in 96-well plates (200 μl/well; approximately 1.5×10^5 cells/well). Three days after transfection, the growth medium was removed, and the cells were washed three times with lithium chloride (10 mM)-supplemented Krebs-Henseleit solution (Krebs-Li) and then incubated with 10^{-9} M [^{3}H]NMS in Krebs-Li solution at 37°C for 1 h to provide estimates of cell-surface receptor expression levels in phosphoinositide turnover assays. Nonspecific binding was determined by the coaddition of 10^{-5} M scopolamine. At the end of the incubation, the cells were rapidly washed a further three times with 3 × 0.2 ml of ice-cold Krebs-Li, solubilized in 100 μl of 1% SDS, and the lysate counted in a Wallac 1409 liquid scintillation counter (PerkinElmer Life and Analytical Sciences). For the wild-type receptor, the mean of the values obtained was 47 ± 9 fmol/assay (mean ± S.D.) corresponding to approximately 2×10^5 [^{3}H]NMS binding sites/cell.

Phosphoinositide Functional Response. G protein activation by the mutant receptors was assessed by measurements of inositol phosphate accumulation in transfected cells grown in 96-well tissue-culture plates as described previously (Lebon et al., 2009). After 24 h, the growth medium was replaced by medium containing [^{3}H]inositol (2.5 μCi/ml), and incubation continued for a further 48 h. Dose-response curves were determined for a full agonist, ACh (10^{-10} to 10^{-3} M), a partial agonist, pilocarpine (10^{-9} to 10^{-2} M), and an inverse agonist, NMS (10^{-11} to 10^{-5} M). In a typical experiment, cells transfected with each of two mutant receptors were compared with a simultaneously transfected wild-type control. Each plate was set up to generate a dose-response curve to ACh, to pilocarpine, and to NMS and to provide a measurement of cell-surface receptor expression using 10^{-9} M [^{3}H]NMS. The cells were pretreated with Krebs-Henseleit solution supplemented with 10 mM LiCl to inhibit inositol monophosphatase activity, for 30 min at 37°C in the presence of 5% CO_2 before the addition of the agonist dilutions in the same medium. The final incubation time was 1 h. Each point on the dose-response curves was determined in triplicate. After aspiration of the medium, accumulated ^{3}H-labeled phosphoinositides were detected in lysates of the cells obtained by adding 200 μl of 0.1 M formic acid to the wells. In a slight variation on the procedure described previously, 40 μl of the lysate was mixed with 80 μl of a 6.5 mg/ml suspension of RNA binding yttrium silicate scintillation proximity assay beads (GE Healthcare). Bound [^{3}H]inositol phosphates were measured in a 1450 MicroBeta TriLux counter using a scintillation proximity assay protocol.

Data Analysis. Radioligand binding curves and functional dose-response curves were analyzed by least-squares fitting using SigmaPlot 10. Radioligand saturation curves were fitted to a depletion-corrected one-site binding model, yielding a pK_d value, and an estimate of the total number of binding sites present in the assay, R_T. The mean expression level of the wild-type receptor was 2.9 ± 1.5 pmol/mg protein (mean ± S.D.). Simultaneous ACh competition curves were globally fitted to an allosteric ternary complex model with the cooperativity parameter set to 10^{-6} representing competi-

tive interactions between [^{3}H]NMS and ACh as described previously (Lebon et al., 2009). These analyses yielded a pK_d value, and a slope factor, usually approximately 0.8. for ACh. Radioligand dissociation data were fitted to a single exponential, as described previously (Goodwin et al., 2007), to estimate a dissociation rate constant.

Phosphoinositide (PI) dose-response curves were fitted to a four-parameter logistic function yielding, for each ligand, a pEC_{50}, a slope factor (close to 1), a basal value, and a maximal response, which was designated $R_{max}A$, $R_{max}P$, or $R_{max}N$, as appropriate for each of the three ligands.

The maximum signal elicited by ACh and pilocarpine was calculated relative to the signal (defined as the 0 signal) measured in the presence of a maximally effective concentration of the inverse agonist, NMS: $S_{max}A = R_{max}A - R_{max}N$; and $S_{max}P = R_{max}P - R_{max}N$. The basal signal was also calculated relative to the 0 signal: S_{bas} = basal $- R_{max}N$. For each set of dose-response curves, the ratios of the maximal to the 0 signals were then calculated; in principle, these ratios should not be sensitive to variations in the cell density and extent of labeling of the phosphoinositide pool: $r_A = S_{max}A/R_{max}N$ and $r_P = S_{max}P/R_{max}N$. The ratio of the pilocarpine maximum signal to the corresponding ACh maximum signal, a measure of pilocarpine signaling efficacy, was then calculated as $e_P = r_P/r_A$. The basal signal elicited by the wild-type and mutant receptors was calculated as a fraction of the maximum ACh-induced response: $E_{bas} = S_{bas}/S_{max}A$. The signaling efficacy of ACh was calculated using an expression published previously (Lu and Hulme, 1999): $e_A = ([K_{act}/K_{bin}(1 - E_{bas})] - 1)/R_T$. In this expression, $K_{act} = 10^{pEC_{50}}$, $K_{bin} = 10^{pK_d}$ (the mean of the values obtained from the ACh binding studies), E_{bas} is as defined above, and R_T is the corresponding cell surface receptor expression level, measured by the [^{3}H]NMS binding capacity (in femtomoles per well) of the cells on the plate.

Statistical Analysis. Determinations were conducted a minimum of three times. Data are presented as mean ± S.E.M. unless otherwise stated. The statistical significance of changes in the mean values of parameters relative to wild-type controls was assessed by one-way analysis of variance followed by Dunnett's post hoc test. Changes in mean values of ratios, relative to an expected value such as 1.0, were assessed using Student's t test.

Construction of a Molecular Model of the M_1 mAChR. The transmembrane domain of the M_1 mAChR was initially modeled on the structure of the high-resolution X-ray crystal structure of the human β_2-adrenergic receptor (PDB code 2RH1; Cherezov et al., 2007). This was highly similar to our previous model (Lu et al., 2001) based on the structure of bovine rhodopsin (PDB code 1F88; Palczewski et al., 2000) in terms of the relative orientation of the seven transmembrane helices. However, the conformation of ECL2 was entirely different, which required care in the retention of the *cis*-disulfide bond between Cys98 and Cys178. Alignment between the M_1 and β_2 sequences was anchored on several motifs: GNXLV in TM1, SLACADL in TM2, DRYF in TM3, WXVS in TM4, FYXP in TM5, FXLXWXP in TM6, and YVNSXXNP in TM7. The crystal structure coordinates were obtained from the Protein Data Bank. The modeling software used was QUANTA (Accelrys, San Diego, CA) running on a Linux-based workstation. The "Modeler" option within QUANTA was used to build 20 models of the M_1 mAChR, including the disulfide bond. The different models were calculated by varying the initial model and optimizing the objective function using conjugate gradients and molecular dynamics with simulated annealing using the CHARMM force field. The model with the lowest objective function was used for further modeling. This consisted of refining ECL3 based on the extracellular loop from the human A_{2A}-adenosine receptor (PDB code 3EML; Jaakola et al., 2008), which contains a homologous pair of cysteine residues that form a disulfide bond and a revised truncation of ICL3 (Δ225–339) based on significant sequence homology to ICL3 from the structure of squid rhodopsin (PDB code 2Z73; Murakami and Kouyama, 2008), which is also G_q-coupled and mediates PI breakdown.

Results

Equilibrium Binding of [^{3}H]NMS. The effects of H8 mutations were evaluated in the context of the rat M_1 mAChR transiently expressed in COS-7 cells. The binding of [^{3}H]NMS to the wild-type M_1 mAChR was described by a single-site binding model with a pK_d of 9.97 ± 0.19 (mean ± S.D.). The mean expression level of the WT receptor was 2.95 ± 0.64 pmol/mg protein (mean ± S.E.M., five independent transfections).

The mutation of residues in the putative H8 of the M_1 mAChR had no significant effect on the affinity of the inverse agonist [^{3}H]NMS, the maximum observed change in the pK_d being a diminution of 0.2 log units. The data are summarized in Supplemental Table 1. Except in the case of N422A, estimates of the membrane expression levels of [^{3}H]NMS binding sites were similar to those of the wild-type, ranging from 40 (D427A) to 212% (L431A) of the control values. A similar range of variation (32–130%) was found when cell-surface

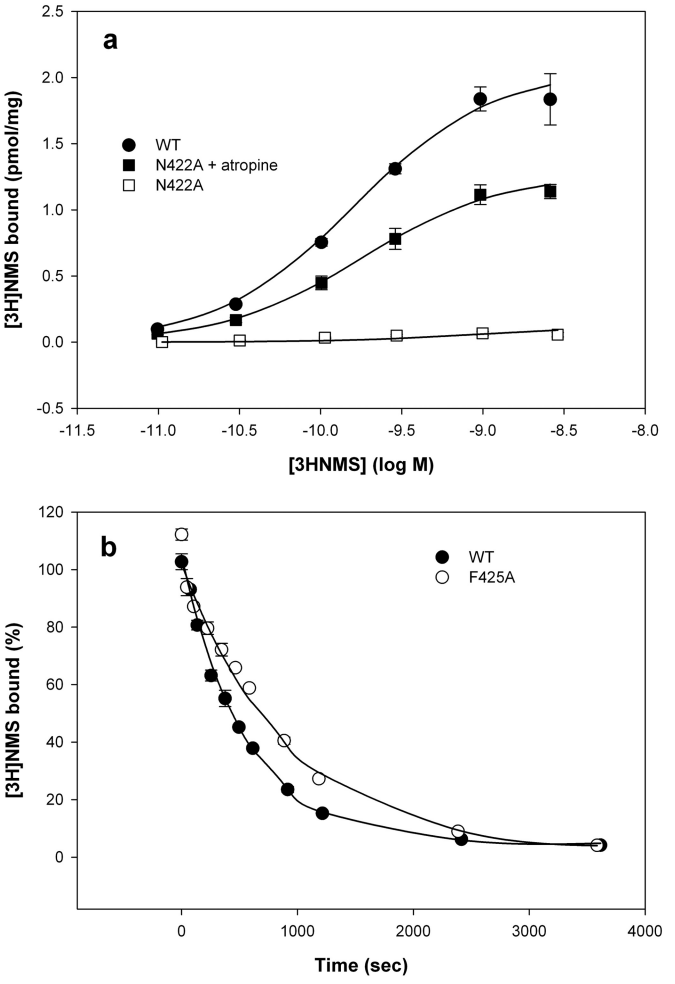

Fig. 1. Representative experiments showing the effects of H8 mutations on the equilibrium binding and dissociation kinetics of [^{3}H]NMS. Wild-type and mutant rat M_1 mAChRs were transiently expressed in COS-7 cells. a, decrease in maximum receptor expression caused by the N422A mutation and its rescue by atropine pretreatment in culture; ●, WT, pK_d = 9.82, R_T = 2.06 pmol/mg; □, N422A pK_d = 9.0; R_T = 0.12 pmol/mg; ■, N422A + atropine, pK_d = 9.76, R_T = 1.28 pmol/mg; full curves are fits to a single-site saturation model of binding. b, retardation of dissociation of [^{3}H]NMS by the F425A mutation; ●, WT, $k_{off} = 1.82 \times 10^{-3}$ s^{-1}; ○, F425A, $k_{off} = 1.09 \times 10^{-3}$ s^{-1}; full curves are fits to a monoexponential function.

receptor expression levels were estimated by [^{3}H]NMS binding to intact cells. Both measures detected somewhat enhanced expression of L431A. These data are summarized in Supplemental Table 2.

In the case of N422A, the expression of specific [^{3}H]NMS binding sites was reduced to approximately 7% of the value of wild-type controls. As reported for other mutations that adversely effect expression levels (Lu and Hulme, 1999; Lu et al., 2001; Bee and Hulme, 2007), the expression of this mutant was enhanced by treatment of the transfected COS-7 cells with 10^{-6} M atropine for 48 h before harvesting, the specific activity increasing from 6 to 62% of a cotransfected WT control for the experiment shown in Fig. 1a. Overall, the mean estimate of the specific activity of N422A in membranes from atropine-pretreated cells was somewhat lower, 34% of the mean specific activity of the wild-type receptor.

Dissociation Kinetics of [^{3}H]NMS. The dissociation of [^{3}H]NMS from the wild-type receptor was adequately described by a monoexponential process with a rate constant of 0.107 ± 0.0012 min^{-1} (mean ± S.D., 1.78 × 10^{-3} s^{-1}), in reasonable agreement with values published previously (Goodwin et al., 2007). Only one of the mutants, F425A, showed an altered rate, with a value of 70% of the wild-type value (Fig. 1b). Because the affinity constant was unaltered, this implies a similarly small reduction in the association

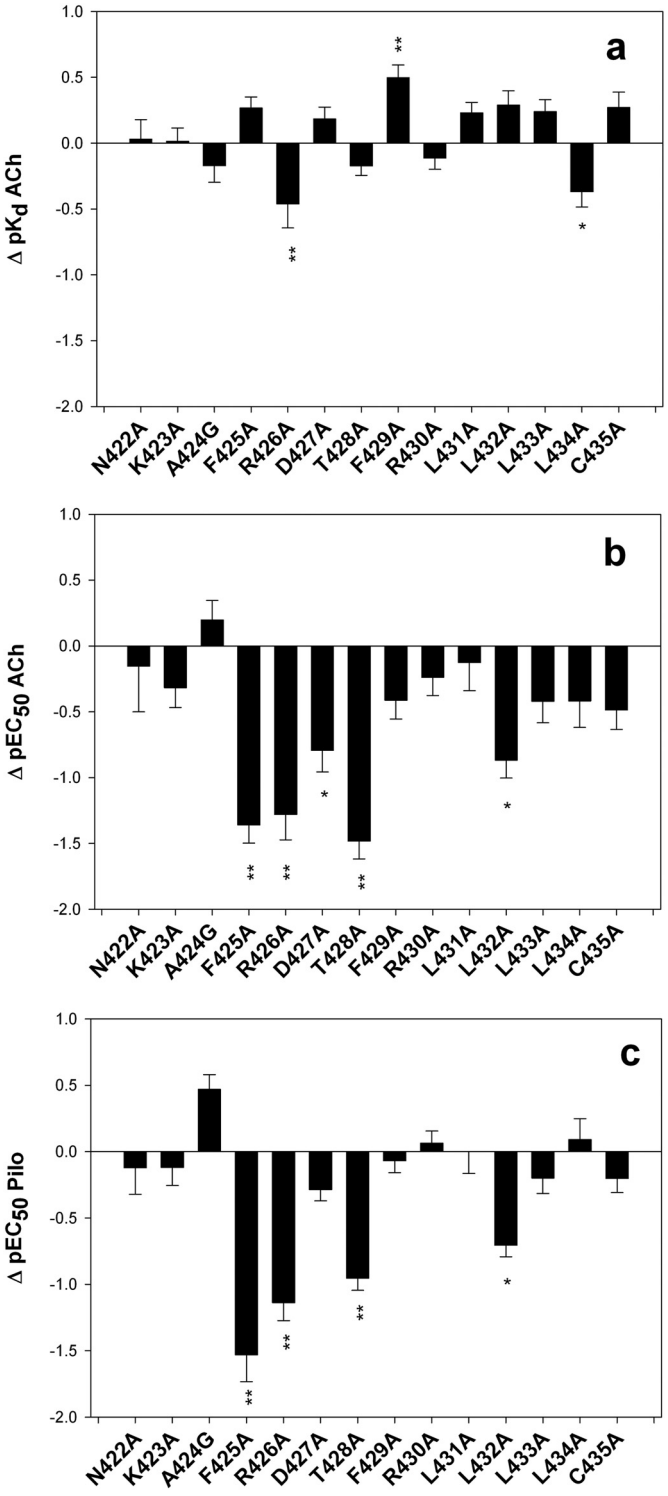

Fig. 2. Summary of effects of mutations of H8 on the binding affinity of ACh (a), on the phosphoinositide signaling potency of ACh (b), and on the potency of pilocarpine (c). Wild-type and mutant rat M_1 mAChRs were transiently expressed in COS-7 cells. Changes relative to wild-type are displayed on a log scale and are shown as mean ± S.E.M. The full data set is given in Supplemental Tables 3 and 4. *, $P < 0.05$; **, $P < 0.01$ with respect to wild type.

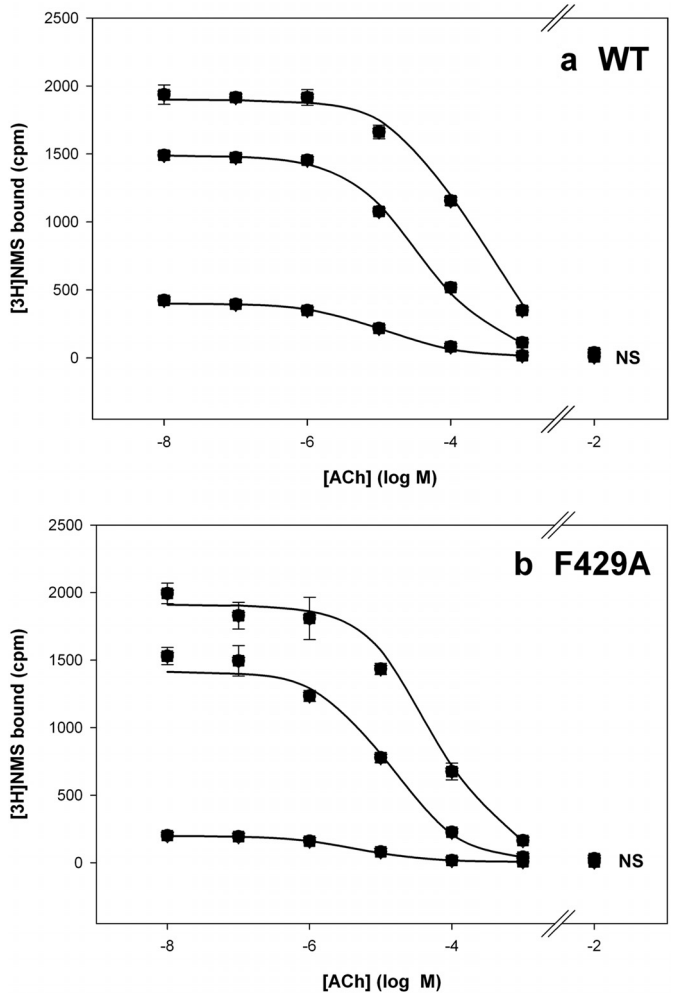

Fig. 3. Representative experiments showing the effect of the F429A mutation on the binding affinity of ACh measured by inhibition of the binding of three concentrations of [^{3}H]NMS. Wild-type and mutant rat M_1 mAChRs were transiently expressed in COS-7 cells. Full curves represent global fits to a competitive model of ACh-[^{3}H]NMS binding. a, WT, pK_d ACh 5.12 ± 0.09 (n_H = 0.84); b, F429A, pK_d, ACh = 5.44 ± 0.06 (n_H = 0.90).

rate constant. The data are summarized in Supplemental Table 1.

Equilibrium Binding of ACh. ACh binding was measured by inhibition of the binding of [^{3}H]NMS. Binding to the wild-type receptor was described by a pK_d of 5.06 ± 0.25 (mean ± S.D.) and a Hill coefficient of approximately 0.8, as found previously (Lu and Hulme, 1999). Most mutations failed to affect the equilibrium affinity of ACh. However, R426A and L434A elicited approximately 3-fold reductions, whereas F429A caused a 3-fold increase in ACh affinity (Fig. 2a), indicating possible effects on the agonist-induced conformational change. Representative experiments are shown in Fig. 3. The data were well described by a competitive model of ACh-[^{3}H]NMS interaction. The data are summarized in Supplemental Table 3.

Phosphoinositide Signaling Response. PI signaling was measured in transfected cells prelabeled with [^{3}H]inositol. Responses to the full agonist, ACh, a partial agonist, pilocarpine, and an inverse agonist, NMS, were measured in each experiment. The response in the presence of a receptor-saturating concentration of NMS was used to define the background level. The data set is summarized in Supplemental Table 4.

As shown in Fig. 4a, ACh elicited a robust PI response from the wild-type M_1 mAChR, with a ratio of stimulated-to-background signaling of 4- to 7-fold and a pEC_{50} of 7.60 ± 0.38 (mean ± S.D.). Pilo elicited a similar maximum response, with a pEC_{50} of 6.08 ± 0.24 (mean ± S.D.). The potencies are in good agreement with previous findings (Page et al., 1995), although in the present experiments, Pilo elicited a maximum response equivalent to that of ACh from the wild-type receptor. The inverse agonist NMS inhibited the basal response of the wild-type receptor by approximately 30% (Fig. 4a). The mean of the NMS- inhibited signal was approximately 13.5% when expressed as a fraction of the ACh-stimulated maximum signal, and the pIC_{50} for NMS was 9.0. A similar effect has been described previously (Goodwin et al., 2007).

Although none of the mutations significantly altered the maximum response to ACh relative to a contemporaneous wild-type control, five of them, F425A, R426A, D427A, T428A, and L432A, significantly reduced the potency of ACh, the effect ranging from 6.3-fold (D427A) to 31-fold (T428A) (Figs. 2b and 4, b and c). Four of the five, the exception being D427A, also reduced the potency of Pilo to a similar extent (Figs. 2c and 4, b and c), and three of these additionally reduced e_P, the maximum signal elicited by Pilo relative to ACh, the fractional values being 31 (F425A), 74 (R426A), and 69% (T428A) indicating a reduction of its signaling efficacy. F425A, R426A, T428A, and L432A showed significantly reduced or undetectable NMS inhibition of the basal PI signal (Supplemental Table 4), as illustrated in Fig. 4, b and c, for F425A and T428A, respectively. In contrast, F429A increased the NMS-inhibited basal activity by approximately 2-fold (Fig. 4d), without any significant change in agonist potencies or the maximum response.

The potency of a full agonist, such as ACh, is dependent on three factors: the binding affinity, the expression level of the receptor relative to the G protein to which it couples, and the signaling efficacy, e_A, of the agonist-receptor complex for the coupled G protein. We have shown that, when the mutation does not reduce the maximum ACh-stimulated response, it is possible to estimate e_A by combining the signaling, binding and receptor expression parameters using the equation described under *Materials and Methods* (Lu and Hulme, 1999).

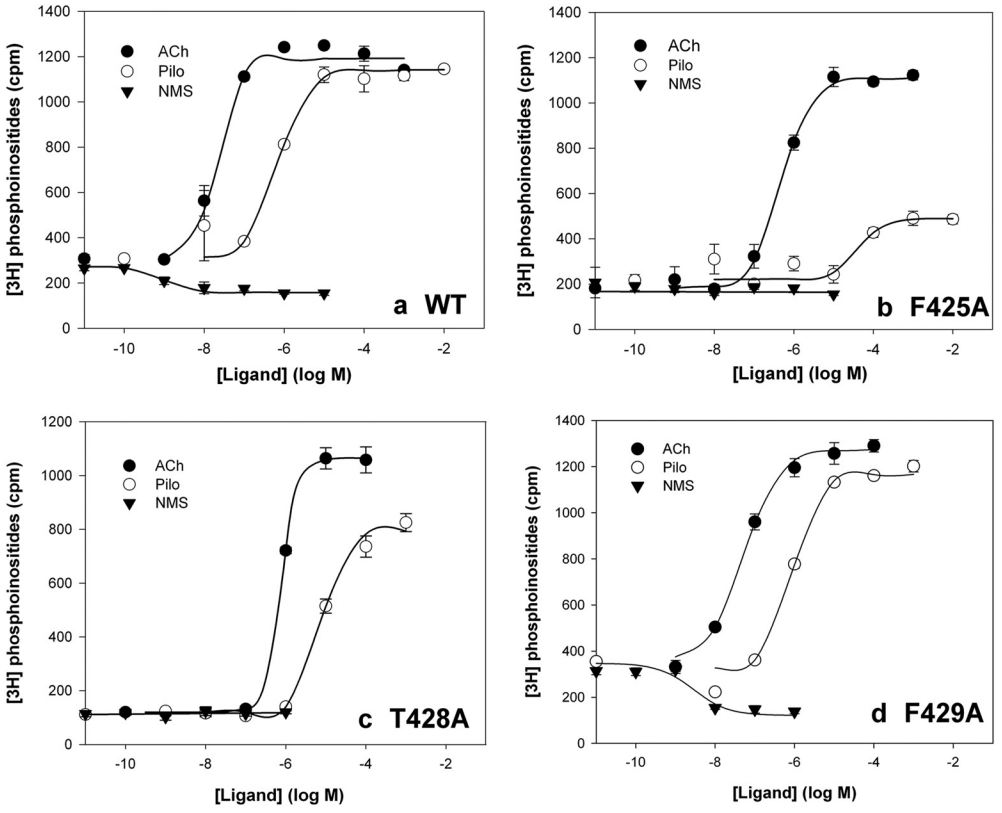

Fig. 4. Representative experiments showing the effects of H8 mutations on the PI signaling response elicited by ACh, pilocarpine, and NMS. Wild-type and mutant rat M_1 mAChRs were transiently expressed in COS-7 cells. Full curves show fits to a logistic function. Results are given as pEC_{50} for ACh, pEC_{50} (e_P) for pilocarpine, and pEC_{50} (E_{bas}) for NMS, where the pilocarpine or NMS responses are given as a fraction of the total ACh-elicited PI signal. N.D., not measurable. Further details are given in Supplemental Table 4. a, wild type, 7.69, 6.16 (0.95), and 9.0 (0.11), respectively; b, F425A, 6.31, 4.37 (0.32), and N.D., respectively; c, T428A, 6.11, 5.09 (0.71), and N.D., respectively; d, F429A, 7.27, 6.04 (0.91), and 8.55 (0.19), respectively.

The results are plotted in Fig. 5a and summarized in Supplemental Table 4.

We have suggested previously that, given the multifactorial nature of e_A, changes should exceed 5-fold to be considered functionally significant. Four of the mutations that reduced ACh potency met this criterion—F425A, R426A, T428A, and L432A—with reductions ranging from 6- to 18-fold. In addition, F429A showed a reduction in e_A approaching 10-fold, reflecting the finding that its signaling potency failed to increase in parallel with its binding affinity. F425A, R426A, and T428A showed parallel decreases in e_P, the maximum Pilo signal relative to that of ACh (Fig. 5b). L432A showed a similar trend, but the change failed to reach statistical significance.

Modeling of the M_1 mAChR. A model of the transmembrane domain of the M_1 mAChR was built by homology with the high-resolution crystal structure of the human β_2-adrenergic receptor. Details of the procedure are described under *Materials and Methods*. Differences to our earlier rhodopsin-based model (Lu et al., 2001) included the remodeling of ECL2 in a more "open" conformation while retaining the *cis*-disulfide bond between Cys98 (TM3) and Cys178 and refinement of ECL3 on the basis of the corresponding loop in the extracellular domain of the A_{2A} adenosine receptor, which contains a homologous pair of cysteine residues that are disulfide bonded (Jaakola et al., 2008). ICL3 incorporated a revised truncation (Δ225–239) designed to retain homologous sequences found in squid rhodopsin, in which they form extensions of TM5 and TM6 that may participate in G_q recognition (Murakami and Kouyama, 2008).

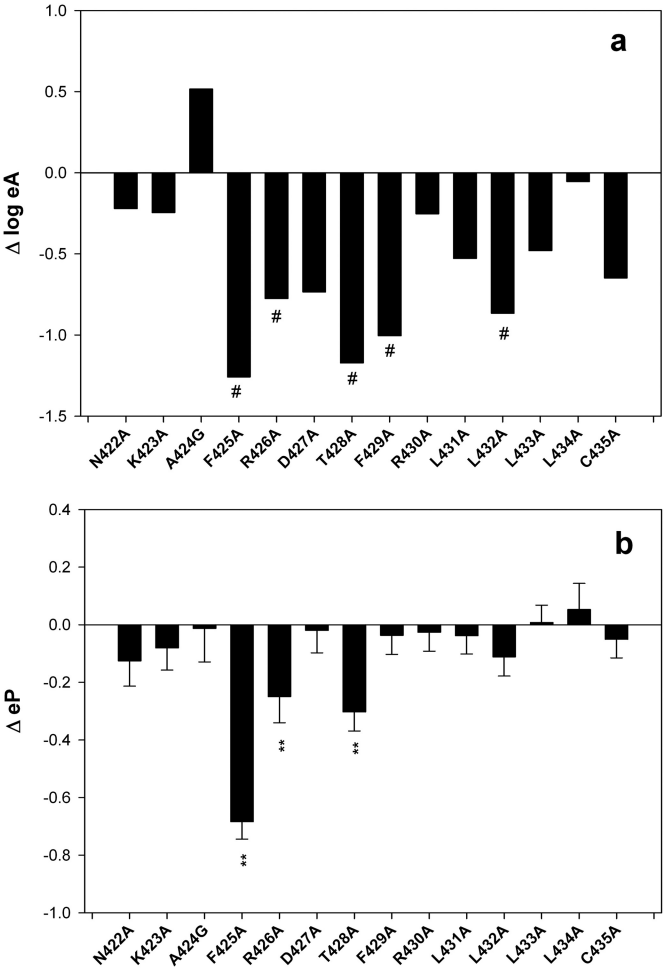

Fig. 5. Changes in ACh and pilocarpine signaling efficacy elicited by H8 mutations. Wild-type and mutant rat M_1 mAChRs were transiently expressed in COS-7 cells. Signaling efficacies were calculated as under *Materials and Methods*. a, ACh: changes in e_A are plotted on a log scale; #, >5-fold ratio relative to the wild type; b, pilocarpine: changes in e_P are plotted; **, $P < 0.01$ with respect to wild type.

A key difference between our revised model of the M_1 mAChR and the original model based on the structure of rhodopsin concerns potential interactions between Tyr418 (7.53) and Phe425 (7.60). In the ground state structure of bovine rhodopsin, the side chain of Tyr7.53 is rotated toward the intracellular surface to form a microdomain, in which the aromatic ring stacks with the side chain of Phe7.60 (Palczewski et al., 2000). In contrast, in squid rhodopsin (Murakami and Kouyama, 2008) and the β_1(Warne et al., 2008) and β_2 (Cherezov et al., 2007) adrenoceptors, the side chain of Tyr7.53 is rotated upward to lie more or less parallel to the side chain of Asn7.49. In our earlier model of the M_1 mAChR (Lu et al., 2002), as in ground state bovine rhodopsin (Fig. 7a), the postulated aromatic stacking interaction also sequesters and restricts the side chain of Phe7.60. In contrast, in the revised model of M_1 (Fig. 7b), like the β_2 adrenoceptor and the active structure of opsin (Fig. 7c), the side chain of Phe7.60 rotates outward about the Cα–Cβ bond, and so becomes accessible to approach from the cytoplasmic surface of the receptor. Related to this conformational difference, in the rhodopsin-based model of M_1, as in rhodopsin itself, the last turn of TM7 corresponding to Ala419 (7.54) to Asn422 (7.57) is substantially unwound. In contrast, in the β_2 adrenoceptor-based model, the corresponding residues are more tightly wound, forming an additional helical turn. This brings the amide side chain of Asn422 into close proximity to the main chain carbonyl group of Ala419, forming a C-cap to TM7 (Fig. 6b). This facilitates the tight turn that allows H8 to depart in an orthogonal direction, emulating the role of Pro330 in the β_2 adrenoceptor (Cherezov et al., 2007). However, no such structural importance attaches to Asn422 in the rhodopsin-based model.

Discussion

The phenotypes of alanine-substitution mutations provide insight into the functional role of the targeted side chain within the receptor structure (Bee and Hulme, 2007; Hulme et al., 2007). H8 is remote from the ligand binding site of the M_1 mAChR and has limited potential for interactions with the core of the transmembrane domain. Only one mutation, N422A, had a destabilizing effect on the receptor structure, reflected in a strongly lowered receptor expression level that could be rescued by the pharmacological chaperone effect of atropine. Likewise, there were only limited effects on the equilibrium binding affinity of NMS and ACh, or on the kinetics of NMS binding.

In a study of TM7, we found that the alanine substitution of Tyr418 (7.53) in the NPXXY switch motif, in addition to causing a large reduction in signaling efficacy, also strongly (30-fold) enhanced ACh affinity, consistent with the ablation of a key intramolecular contact that stabilizes the inactive ground state as opposed to the ACh-activated state of the receptor (Lu et al., 2001). Molecular modeling based on the ground state structure of bovine rhodopsin suggested that

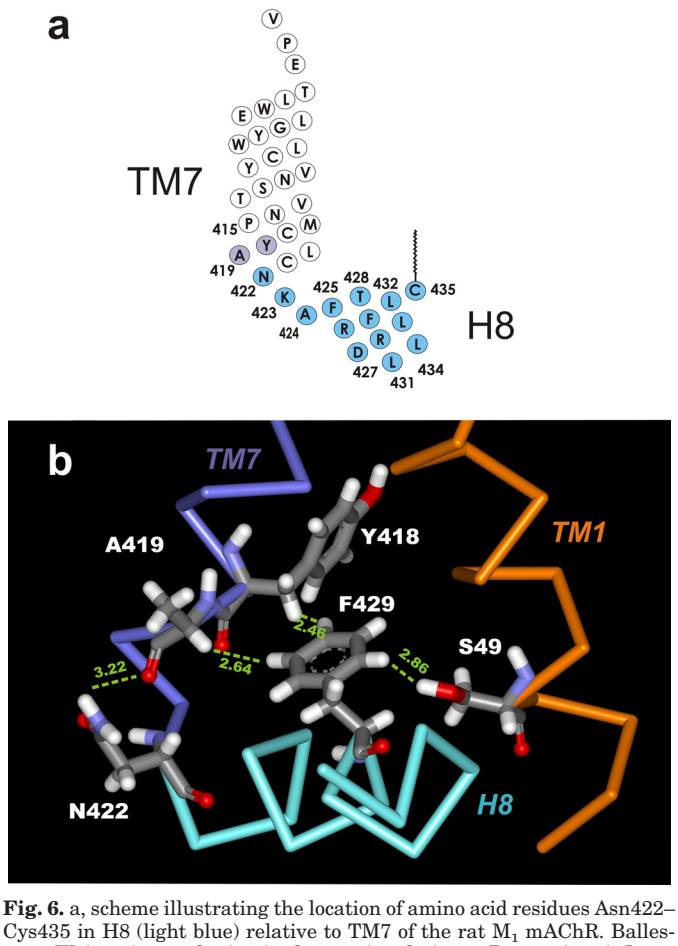

Fig. 6. a, scheme illustrating the location of amino acid residues Asn422–Cys435 in H8 (light blue) relative to TM7 of the rat M_1 mAChR. Ballesteros-Weinstein numbering in the text is relative to Pro415 (7.50). Locations of Tyr418 (7.53) and Ala419 (7.54) are also shown (mauve). The wavy line represents the putative palmitoylation site. b, interactions of Asn422 and Phe429 within a homology model of the M_1 mAChR. The C-terminal ends of TM1 (brown) and TM7 (mauve) are shown, along with the interface between TM7 and H8 (residues Asn422–Cys435, cyan). The rest of the structure has been omitted for clarity. The view is from outside the helix bundle, parallel to the plane of the membrane, defined by the top surface of H8. The amide group of Asn422 "caps" the C terminus of TM7 by bonding to the backbone carbonyl of Ala419, stabilizing the turn between TM7 and H8. The aromatic ring of Phe429 helps to position H8 with respect to TM7 (Tyr418, Ala419) and TM1 (Ser49). Distances (dotted lines) are in angstroms.

this contact might be with the aromatic ring of Phe425 (7.60) (Lu et al., 2002). However, the absence of any corresponding increase in ACh affinity in the F425A mutant suggests that this stacking contact does not exist in the unliganded M_1 mAChR. Indeed, it has not been found in the crystal structures of the antagonist complexes of the β_1 and β_2 adrenoceptors, the A_{2A} adenosine receptor, and squid rhodopsin; in all of these structures, Tyr7.53 is in a different rotameric state to that found in bovine rhodopsin. Interestingly, the F429A mutation did show a modest enhancement of ACh affinity accompanied by somewhat increased basal signaling activity and decreased signaling efficacy, a phenotype similar to that of Y418A.

The locations of the residues mutated in this study are indicated in the scheme shown in Fig. 6a. A molecular model of the TM domain and H8 of the M_1 mAChR based on homology to the β_2-adrenergic receptor and the G_q-coupled squid rhodopsin provides a plausible explanation for the roles of Asn422 and Phe429 within this sequence (Fig. 6b). The amide group of Asn422 interacts with the carbonyl group of Ala419 (7.54), thus acting as a C-cap to TM7, and stabilizing the turn that allows H8 to depart in a different direction. Alanine substitution of Asn422 would remove this bond, destabilizing the junction. Within 2.46 to 2.86 Å of the phenyl ring of Phe429 are the α-proton of Ala419 (7.54), the β-proton of Tyr418 (7.53), and the hydroxyl group of Ser49 (1.56). These contacts of Phe429 may help to restrict movements of TM7 relative to H8 in the ground state of the receptor. Activation involves a large movement of the side chain of Tyr7.53 (Scheerer et al., 2008). The ring of Phe429 may also be involved in building the active state conformation, as evidenced by the significant loss of ACh signaling efficacy that accompanied its alanine substitution.

The main finding was the identification of four more residues whose alanine substitution caused a substantial decrease in signaling efficacy, namely Phe425, Arg426, Thr428, and Leu432. The periodic variation in potency, with the effect peaking every fourth residue (Fig. 2c), is compatible with the proposed α-helical structure for this sequence, at least in the activated state of the receptor. In only one case, R426A, was there any measurable decrease in ACh affinity, which is believed to reflect perturbation of the G protein independent ground state. Thus, their phenotype suggests that these res-

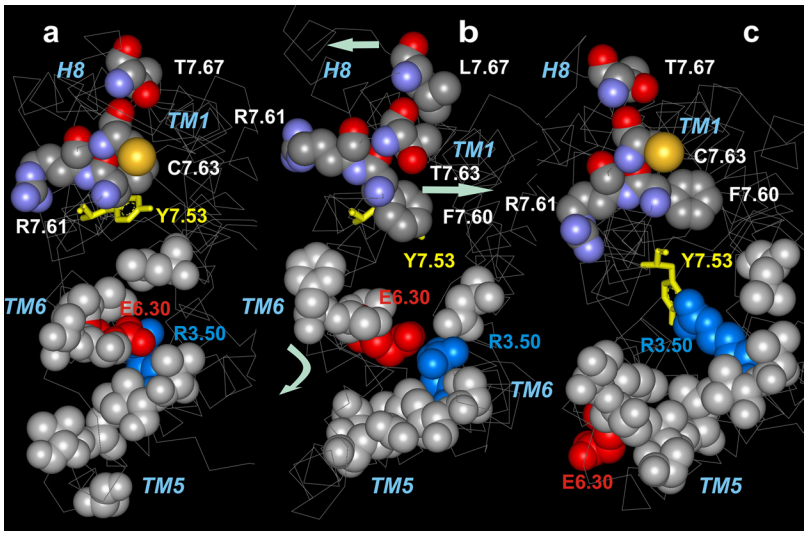

Fig. 7. Proposed G protein contact residues in H8 [Corey/Pauling/Koltun (CPK) format colored by element and labeled in white using Ballesteros-Weinstein numbering], and elsewhere (CPK format colored gray) in bovine rhodopsin (PDB 1GZM; Li et al., 2004) (a), the M_1 mAChR homology model (*Materials and Methods*) (b), and the bovine opsin-transducin peptide complex (c) (PDB 3DQB; Scheerer et al., 2008; the transducin peptide has been omitted for clarity). The gray-colored atoms are those belonging to contact residues for the transducin C-terminal peptide in its complex with opsin (c) and their homologs in ground-state rhodopsin (a) and the M_1 mAChR (b). A key contact residue is Arg3.50 (blue), which forms an "ionic lock" with Glu6.30 (red) in ground-state rhodopsin (a). The residues colored by element are those identified in this study as important for PI signaling in H8 of the M_1 mAChR (b) and their homologs in rhodopsin (a) and opsin-transducin (c). Tyr7.53 of the NPXXY switch sequence in TM7 is also shown. All of the views are directed toward the cytoplasmic loops of the receptors, normal to the plane of the membrane. The position of the cytoplasmic terminus of TM1 is also indicated, as are TM5 and TM6. The arrows indicate rotational movements of TM6 and H8 that may accompany transition to the active state.

idues may be directly involved in G_q binding in the agonist-induced signaling state of the M_1 mAChR. It should be noted, however, that the maximum effect on efficacy, 18-fold, was significantly less than the 100-fold decrease that resulted from the mutation of the conserved Arg3.50 that is believed to play a critical part in anchoring the C terminus of the G protein (Jones et al., 1995; Scheerer et al., 2008). It is noteworthy that alanine substitution of the putatively palmitoylated Cys432 did not affect signaling. A similar observation has been made for serine substitution of this residue (Savarese et al., 1992).

Mapping these residues onto the model of the M_1 mAChR shows that three of them, Phe425 (7.60), Thr428 (7.63), and Leu432 (7.67) are located on sequential turns in one quadrant of H8, with their side chains projecting parallel to the plane of the lipid bilayer along a vector oriented toward TM1, whereas the fourth, Arg426 (7.61), is on the opposite, outward face of the helix (Fig. 7b). Also shown in the model are the locations of the M_1 mAChR residues homologous to the contact residues for the C-terminal peptide of $G_t\alpha$ in the crystal structure of its complex with "activated" acid opsin (Scheerer et al., 2008) and the "ionic lock" residues Arg3.50 and Glu6.30.

In the ground state of rhodopsin (Li et al., 2004), Phe7.60 is stacked with, and restricts, Tyr7.53. Likewise, the other G-protein recognition residues are held in a compact configuration by the ionic lock (Fig. 7a). It is noteworthy that in contrast to the M_1 mAChR, rhodopsin has no detectable basal signaling activity (Hofmann et al., 2009). In the "active" $G_t\alpha$-opsin complex, the ionic lock is broken, allowing TM6 to rotate and swing out (Fig. 7c). The contact between Phe7.60 and Tyr7.53 is broken, allowing the side chain of the latter to swing around to underpin the key contact made by Arg3.50 with a β-turn near the C terminus of the $G_t\alpha$ peptide, and H8 rotates around an axis normal to the plane of the membrane. The recognition residues in TM5 and TM6 click into register with the H8 residues to form an extended surface for G protein recognition. According to this view, the unliganded M_1 mAChR exists in an intermediate, partly activated conformation, which is consistent with its possession of significant basal signaling activity.

That agonist binding induces a conformational change involving H8 was suggested by a cysteine substitution and induced disulfide cross-linking study on the M_3 mAChR (Li et al., 2007). Increased spatial separation or conformational mobility between the N-terminal segment of H8 and TM1 is a favored interpretation. An extension of this study demonstrated facile cross-linking of cysteine residues substituted for the last three amino acids of $G_q\alpha$ to M_3 mutants at positions corresponding to Lys423 (7.58), Ala424 (7.59), Asp427 (7.62), and Leu431 (7.66), which are adjacent to the signal transduction-critical positions that we have identified (Fig. 6a) but instead point directly into the cytoplasm (Hu et al., 2010). Cross-linking was particularly strong at positions 7.62 and 7.66 and was independent of agonist activation. In contrast, agonist-dependent cross-links were formed between the C-terminal residues of $G_q\alpha$ and a position in TM6 demonstrated previously to be involved in G protein-specificity (Blin et al., 1995) and between a residue in the α4-β6 loop of $G_q\alpha$ and positions 7.58, 7.59, and 7.62 in H8.

Based on these studies, an attractive hypothesis is that the membrane-associated H8 helix acts as an initial docking station for the C-terminal helix of $G_q\alpha$ when an encounter complex is formed between the receptor and the membrane-anchored G protein heterotrimer. Under the influence of the agonist, opening of the cytoplasmic surface of the receptor may allow the $G_q\alpha$ C terminus to migrate to its final position within the core of the TM bundle. The extension of the G_q binding domain into H8, suggested by the present study, may then integrate other elements of the G protein, such as the α4–β6 loop of the α subunit, into the active ternary complex.

Acknowledgments

We are grateful to Carol Curtis for expert technical assistance, advice, and support.

Authorship Contributions

Participated in research design: Lu and Hulme.
Conducted experiments: Kaye.
Contributed new reagents or analytic tools: Saldanha and Lu.
Performed data analysis: Kaye and Hulme.
Wrote or contributed to the writing of the manuscript: Kaye, Saldanha, Lu, and Hulme.

References

Altenbach C, Cai K, Khorana HG, and Hubbell WL (1999) Structural features and light-dependent changes in the sequence 306–322 extending from helix VII to the palmitoylation sites in rhodopsin: a site-directed spin-labeling study. *Biochemistry* **38:**7931–7937.

Anavi-Goffer S, Fleischer D, Hurst DP, Lynch DL, Barnett-Norris J, Shi S, Lewis DL, Mukhopadhyay S, Howlett AC, Reggio PH, et al. (2007) Helix 8 Leu in the CB1 cannabinoid receptor contributes to selective signal transduction mechanisms. *J Biol Chem* **282:**25100–25113.

Bee MS and Hulme EC (2007) Functional analysis of transmembrane domain 2 of the M1 muscarinic acetylcholine receptor. *J Biol Chem* **282:**32471–32479.

Blin N, Yun J, and Wess J (1995) Mapping of single amino acid residues required for selective activation of Gq/11 by the m3 muscarinic acetylcholine receptor. *J Biol Chem* **270:**17741–17748.

Cai K, Klein-Seetharaman J, Farrens D, Zhang C, Altenbach C, Hubbell WL, and Khorana HG (1999) Single-cysteine substitution mutants at amino acid positions 306–321 in rhodopsin, the sequence between the cytoplasmic end of helix VII and the palmitoylation sites: sulfhydryl reactivity and transducin activation reveal a tertiary structure. *Biochemistry* **38:**7925–7930.

Cherezov V, Rosenbaum DM, Hanson MA, Rasmussen SG, Thian FS, Kobilka TS, Choi HJ, Kuhn P, Weis WI, Kobilka BK, et al. (2007) High-resolution crystal structure of an engineered human beta2-adrenergic G protein-coupled receptor. *Science* **318:**1258–1265.

Delos Santos NM, Gardner LA, White SW, and Bahouth SW (2006) Characterization of the residues in helix 8 of the human beta1-adrenergic receptor that are involved in coupling the receptor to G proteins. *J Biol Chem* **281:**12896–12907.

Fritze O, Filipek S, Kuksa V, Palczewski K, Hofmann KP, and Ernst OP (2003) Role of the conserved NPxxY(x)5,6F motif in the rhodopsin ground state and during activation. *Proc Natl Acad Sci USA* **100:**2290–2295.

Fung JJ, Deupi X, Pardo L, Yao XJ, Velez-Ruiz GA, Devree BT, Sunahara RK, and Kobilka BK (2009) Ligand-regulated oligomerization of beta(2)-adrenoceptors in a model lipid bilayer. *EMBO J* **28:**3315–3328.

Goodwin JA, Hulme EC, Langmead CJ, and Tehan BG (2007) Roof and floor of the muscarinic binding pocket: variations in the binding modes of orthosteric ligands. *Mol Pharmacol* **72:**1484–1496.

Hoersch D, Otto H, Wallat I, and Heyn MP (2008) Monitoring the conformational changes of photoactivated rhodopsin from microseconds to seconds by transient fluorescence spectroscopy. *Biochemistry* **47:**11518–11527.

Hofmann KP, Scheerer P, Hildebrand PW, Choe HW, Park JH, Heck M, and Ernst OP (2009) A G protein-coupled receptor at work: the rhodopsin model. *Trends Biochem Sci* **34:**540–552.

Hu J, Wang Y, Zhang X, Lloyd JR, Li JH, Karpiak J, Costanzi S, and Wess J (2010) Structural basis of G protein-coupled receptor-G protein interactions. *Nat Chem Biol* **6:**541–548.

Hulme EC, Bee MS, and Goodwin JA (2007) Phenotypic classification of mutants: a tool for understanding ligand binding and activation of muscarinic acetylcholine receptors. *Biochem Soc Trans* **35:**742–745.

Hulme EC, Birdsall NJ, and Buckley NJ (1990) Muscarinic receptor subtypes. *Annu Rev Pharmacol Toxicol* **30:**633–673.

Jaakola VP, Griffith MT, Hanson MA, Cherezov V, Chien EY, Lane JR, Ijzerman AP, and Stevens RC (2008) The 2.6 angstrom crystal structure of a human A2A adenosine receptor bound to an antagonist. *Science* **322:**1211–1217.

Jones PG, Curtis CA, and Hulme EC (1995) The function of a highly-conserved arginine residue in activation of the muscarinic M1 receptor. *Eur J Pharmacol* **288:**251–257.

König B, Arendt A, McDowell JH, Kahlert M, Hargrave PA, and Hofmann KP (1989) Three cytoplasmic loops of rhodopsin interact with transducin. *Proc Natl Acad Sci USA* **86:**6878–6882.

Lebon G, Langmead CJ, Tehan BG, and Hulme EC (2009) Mutagenic mapping suggests a novel binding mode for selective agonists of M1 muscarinic acetylcholine receptors. *Mol Pharmacol* **75:**331–341.
Li J, Edwards PC, Burghammer M, Villa C, and Schertler GF (2004) Structure of bovine rhodopsin in a trigonal crystal form. *J Mol Biol* **343:**1409–1438.
Li JH, Han SJ, Hamdan FF, Kim SK, Jacobson KA, Bloodworth LM, Zhang X, and Wess J (2007) Distinct structural changes in a G protein-coupled receptor caused by different classes of agonist ligands. *J Biol Chem* **282:**26284–26293.
Lu ZL and Hulme EC (1999) The functional topography of transmembrane domain 3 of the M1 muscarinic acetylcholine receptor, revealed by scanning mutagenesis. *J Biol Chem* **274:**7309–7315.
Lu ZL, Saldanha JW, and Hulme EC (2001) Transmembrane domains 4 and 7 of the M(1) muscarinic acetylcholine receptor are critical for ligand binding and the receptor activation switch. *J Biol Chem* **276:**34098–34104.
Lu ZL, Saldanha JW, and Hulme EC (2002) Seven-transmembrane receptors: crystals clarify. *Trends Pharmacol Sci* **23:**140–146.
Milligan G, Parenti M, and Magee AI (1995) The dynamic role of palmitoylation in signal transduction. *Trends Biochem Sci* **20:**181–187.
Murakami M and Kouyama T (2008) Crystal structure of squid rhodopsin. *Nature* **453:**363–367.
O'Dowd BF, Hnatowich M, Caron MG, Lefkowitz RJ, and Bouvier M (1989) Palmitoylation of the human beta 2-adrenergic receptor. Mutation of Cys341 in the carboxyl tail leads to an uncoupled nonpalmitoylated form of the receptor. *J Biol Chem* **264:**7564–7569.
Okuno T, Ago H, Terawaki K, Miyano M, Shimizu T, and Yokomizo T (2003) Helix 8 of the leukotriene B4 receptor is required for the conformational change to the low affinity state after G-protein activation. *J Biol Chem* **278:**41500–41509.
Ovchinnikov YuA, Abdulaev NG, and Bogachuk AS (1988) Two adjacent cysteine residues in the C-terminal cytoplasmic fragment of bovine rhodopsin are palmitylated. *FEBS Lett* **230:**1–5.
Page KM, Curtis CA, Jones PG, and Hulme EC (1995) The functional role of the binding site aspartate in muscarinic acetylcholine receptors, probed by site-directed mutagenesis. *Eur J Pharmacol* **289:**429–437.
Palczewski K, Kumasaka T, Hori T, Behnke CA, Motoshima H, Fox BA, Le Trong I, Teller DC, Okada T, Stenkamp RE, et al. (2000) Crystal structure of rhodopsin: A G protein-coupled receptor. *Science* **289:**739–745.
Prioleau C, Visiers I, Ebersole BJ, Weinstein H, and Sealfon SC (2002) Conserved helix 7 tyrosine acts as a multistate conformational switch in the 5HT2C receptor. Identification of a novel "locked-on" phenotype and double revertant mutations. *J Biol Chem* **277:**36577–36584.
Resek JF, Farahbakhsh ZT, Hubbell WL, and Khorana HG (1993) Formation of the meta II photointermediate is accompanied by conformational changes in the cytoplasmic surface of rhodopsin. *Biochemistry* **32:**12025–12032.
Sano T, Ohyama K, Yamano Y, Nakagomi Y, Nakazawa S, Kikyo M, Shirai H, Blank JS, Exton JH, and Inagami T (1997) A domain for G protein coupling in carboxyl-terminal tail of rat angiotensin II receptor type 1A. *J Biol Chem* **272:**23631–23636.
Savarese TM, Wang CD, and Fraser CM (1992) Site-directed mutagenesis of the rat m1 muscarinic acetylcholine receptor. Role of conserved cysteines in receptor function. *J Biol Chem* **267:**11439–11448.
Sawyer GW, Ehlert FJ, and Shults CA (2010) A conserved motif in the membrane proximal C-terminal tail of human muscarinic m1 acetylcholine receptors affects plasma membrane expression. *J Pharmacol Exp Ther* **332:**76–86.
Scheerer P, Park JH, Hildebrand PW, Kim YJ, Krauss N, Choe HW, Hofmann KP, and Ernst OP (2008) Crystal structure of opsin in its G-protein-interacting conformation. *Nature* **455:**497–502.
Swift S, Leger AJ, Talavera J, Zhang L, Bohm A, and Kuliopulos A (2006) Role of the PAR1 receptor 8th helix in signaling: the 7-8-1 receptor activation mechanism. *J Biol Chem* **281:**4109–4116.
Warne T, Serrano-Vega MJ, Baker JG, Moukhametzianov R, Edwards PC, Henderson R, Leslie AG, Tate CG, and Schertler GF (2008) Structure of a beta1-adrenergic G-protein-coupled receptor. *Nature* **454:**486–491.
Wu B, Chien EY, Mol CD, Fenalti G, Liu W, Katritch V, Abagyan R, Brooun A, Wells P, Bi FC, et al. (2010) Structures of the CXCR4 chemokine GPCR with small-molecule and cyclic peptide antagonists. *Science* **330:**1066–1071.

Address correspondence to: Dr. E. C. Hulme, Division of Physical Biochemistry, MRC National Institute for Medical Research, Mill Hill, London NW7 1AA, United Kingdom. E-mail: ehulme@nimr.mrc.ac.uk